Pergamon

Journal of Structural Geology, Vol. 16, No. 8, pp. 1061 to 1075, 1994

0191-8141/94 $07.00+0.00

0191-8141(93)E0011-9

Geometry and kinematics of active normal faults, South Oquirrh Mountains, Utah: implication for fault growth

DANING WU and RONALD L. BRUHN

Department of Geology and Geophysics, University of Utah, Salt Lake City, UT 84112, U.S.A.

(*Received* 14 *April* 1993; *accepted in revised form* 4 *November* 1993)

Abstract—The NNW-striking South Oquirrh Mountains normal fault zone consists of four individual faults. The individual faults are arranged in a right-stepping pattern in the north and a left-stepping pattern in the south, forming a convex-shaped fault zone in map view with the apex towards the hanging wall. Late Quaternary fault activity is characterized by 2.0–4.5 m high discontinuous fault scarps developed in both late Quaternary alluvium and bedrock. The fault scarps in bedrock contain evidence of two large rupture events. The last large earthquake occurred prior to the highstand of the Bonneville lake cycle (15 ka), based on cross-cutting relationship between the Bonneville shoreline and the fault scarp, and on comparisons of fault scarp morphology. Cumulative displacement patterns inferred from range crest elevations, Bouguer gravity data in the adjacent basin and rotation of the subsidiary faults adjacent to the West Mercur fault are similar to the pattern of displacements measured across late Quaternary fault scarps; that is, the maximum displacement is near the apex of the convex-shaped fault zone, where the West Mercur fault is located, and then tapers off towards both ends of the fault zone. Fault traces that range from a few meters to tens of kilometers long are characterized by two dominant orientations (strike N11°W and N43°W): the two orientations are separated from each other by a statistically constant angle of 33° ± 3°. Slip directions concentrate on a trend of S70°W for both groups of faults, perpendicular to the average strike of the fault zone. These data indicate that the geometry of the fault surfaces is non-cylindrical and may be composed of self-similar structural ridges and troughs of variable wavelength and amplitude that are elongated parallel to slip direction.

The relationships between fault geometry, displacement and geomorphology in the South Oquirrh Mountains fault zone suggests a growth model of normal faults in which apex points on the convex-shaped fault sections mark the nucleation points of primary faults. Secondary faults developed at the ends of the primary fault step into the footwall block as the fault zone grows laterally. Intersecting regions between two laterally growing fault zones are concave-shaped in map view.

INTRODUCTION

ASSESSMENT of fault-associated mineral deposits and of seismic hazards relies partly on a basic understanding of fault behavior. Structural studies of fault-controlled mineral deposits and earthquake ruptures suggest that the mechanical and fluid transport properties of faulting are affected by complexities in fault geometry, such as changes in strike, fault bifurcations and stepovers. Some studies indicate that the geometrical complexity of fault traces observed at the surface may persist downward through the middle crust (Gilluly 1932, Eaton *et al.* 1970, Bakun *et al.* 1980, Reasenberg & Ellsworth 1982, Guilbert & Park 1986, Okubo & Aki 1987). Studies of active normal faults in the Basin and Range Province and Rocky Mountains of the western United States indicate that rupture characteristics are partly related to fault geometry (Slemmons 1957, Wallace 1984, Bruhn *et al.* 1987, Crone & Haller 1991, Machette *et al.* 1991). In particular, spatial correlations are noted between points of rupture nucleation and termination, direction of rupture propagation, and the geometry of fault traces (Sibson 1985, 1987, Bruhn *et al.* 1987). However, methods for inferring the subsurface structure of faults and the manner in which fault zones grow based on interpretation of surficial geological data have received less attention. Here we discuss the use of surficial geologic data to infer the geometry, rupture properties, and evolution of a fault zone in Utah.

A 25 km long active normal fault zone is located along the western flank of the southern Oquirrh Mountains in north-central Utah. This fault zone was partly explored by extensive mining in the early part of the century, and young fault scarps along the mountain front are well preserved, making this an excellent location to study the relationship between fault geometry and kinematics. We first document the geometric and displacement characteristics of the fault zone, and then discuss the evolution of the fault zone based on inferences made from analysis of fault geometry.

GEOLOGIC SETTING

The Oquirrh Mountains are located in north-central Utah, 35 km west of the Wasatch fault zone which forms the physiographic boundary between the Basin and Range Province and the Rocky Mountains. The Oquirrh Mountains are about 50 km long and are part of a belt of N-trending mountain ranges separated by intervening lowlands (Fig. 1). The Oquirrh Mountains are underlain mostly by Paleozoic limestone, dolomite, and interbedded sandstone and shale that are locally intruded by Tertiary igneous rocks and overlain by patches of Ter-

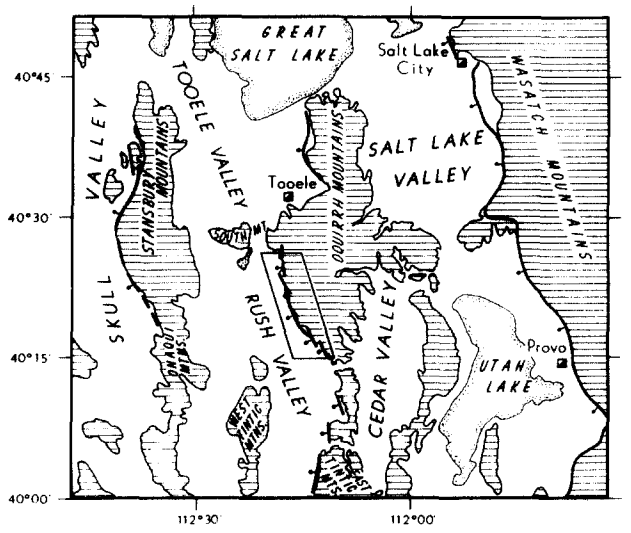

Fig. 1. Location map of study area. Box indicates the southern Oquirrh Mountains area. Bold solid lines indicate active normal faults.

tiary volcanic rocks. The Paleozoic rocks are folded into NNW-trending anticlines and synclines of Mesozoic age (Gilluly 1928, 1929, 1932).

NNW-striking normal faults bound the western flank of the Oquirrh Mountains and control development of the valleys and underlying basins on the west side of the mountains (Fig. 1). Tooele Valley is located adjacent to the western flank of the northern Oquirrh Mountains, and is underlain by a sedimentary basin. The basement of the basin is as deep as 4–5 km and continues north of the range beneath Great Salt Lake (Zoback 1983, Cook *et al.* 1989). South Mountain is an E-trending ridge of Paleozoic bedrock that forms the boundary between Tooele Valley and Rush Valley, a topographic depression separating the Oquirrh and East Tintic Mountains from the Stansbury, Onaqui and West Tintic Mountains. This study focuses on the zone of normal faults located along the eastern side of Rush Valley, which we refer to as the South Oquirrh Mountains fault zone (SOMFZ). This fault zone cuts the western limb of the Ophir anticline, the dominant structure in the southwestern Oquirrh Range (Gilluly 1932).

There is no direct evidence for when the South Oquirrh Mountains fault zone first formed, but normal faulting probably started no early than 12 million years, the age of Salt Lake Group basalt which was the youngest rock offset by normal faults in adjacent areas (J. Helm personal communication 1993). The major phase of normal faulting is believed to have begun between the Miocene and Pliocene when E–W extension was dominant in the eastern Basin and Range region (Rigby 1958, Gilluly 1967, Wright 1977, Zoback 1983).

GENERAL CHARACTERISTICS OF THE SOUTH OQUIRRH MOUNTAINS FAULT ZONE

NNW-striking normal faults are exposed for about 25 km along the western flank of the southern Oquirrh Mountains (Fig. 2a). This fault belt is convex toward the west in map view and comprises four individual faults: the Soldier Canyon fault (SCF), Lakes of Killarney fault (LKF), West Mercur fault (WMF) and West Eagle Hill fault (WEHF). The faults partly overlap one another and are arranged in an échelon pattern (Fig. 2a). The Soldier Canyon and Lakes of Killarney faults are arranged in a right-stepping pattern with respect to the West Mercur fault, but farther south the West Eagle Hill fault is arranged in a left-stepping pattern relative to the West Mercur fault. The faults are longer in the central part of the fault zone and shorter at the ends.

The Soldier Canyon fault is 5 km long, strikes N15°–30°W and dips 65°W based on the measurement of fault surfaces exposed in bedrock on the lower slope of the southern Oquirrh Mountains. The Soldier Canyon fault offsets the upper Mississippian Great Blue Limestone by 800–1000 m south of Soldier Canyon. Fault scarps developed in bedrock during the last one or two earthquakes are 0.5–1.5 m high. The age of these scarps is uncertain, but they are probably late Quaternary because the exposed fault surfaces in the limestone contain striations, unconsolidated breccia and polished furrows which are susceptible to weathering.

The Lakes of Killarney fault is 7 km long, strikes N20°–35°W and dips 65°W near the surface. The fault zone is located about 2 km west of the Soldier Canyon fault, in a right-stepping pattern (Fig. 2a). Along the Lakes of Killarney fault, Quaternary alluvium is faulted directly against bedrock in the most northern section of the fault, but in the southern section the fault extends into bedrock on the flanks of the mountain range (LKF(N) and LKF(S) in Fig. 2a). Evidence for Late Quaternary displacement is confined to the northern section of the fault where a few scarps are located in bedrock, 10–20 m above the contact between Paleozoic limestone and Quaternary alluvium. These fault scarps are 2.5–3.2 m high in limestone, and the morphology of the scarps indicates they were formed during at least two paleo-earthquakes. At several localities the lower part of the scarp is partly polished and contains slicken lines, grooves and breccia. The upper part is eroded in a band about 0.5–0.8 m high, and the limestone surface is rough and solution pitted (Fig. 3). We interpret this morphology to indicate that the upper, weathered band was uplifted during an earthquake, subsequently weathered, and then uplifted again during a younger earthquake. The youngest event formed the less weathered fault surface on the lower part of the scarp.

The Lakes of Killarney fault splits into two branches about 2.0 km north of Dry Canyon (Fig. 2a). The western branch (LKF(W)) is located along the mountain front and has controlled deposition of Quaternary alluvium north of Ophir Canyon. The partly eroded bedrock fault scarp in this branch is 10–15 m high and locally cuts through late Quaternary alluvial fans, where the scarps are only 2.0–3.0 m high (Table 1). The trace of the eastern branch of the fault trends N35°W and cuts into the bedrock before terminating in the southern wall of Ophir Canyon (Fig. 2a). Paleozoic rocks are offset vertically at least 1300–1500 m by the eastern branch of

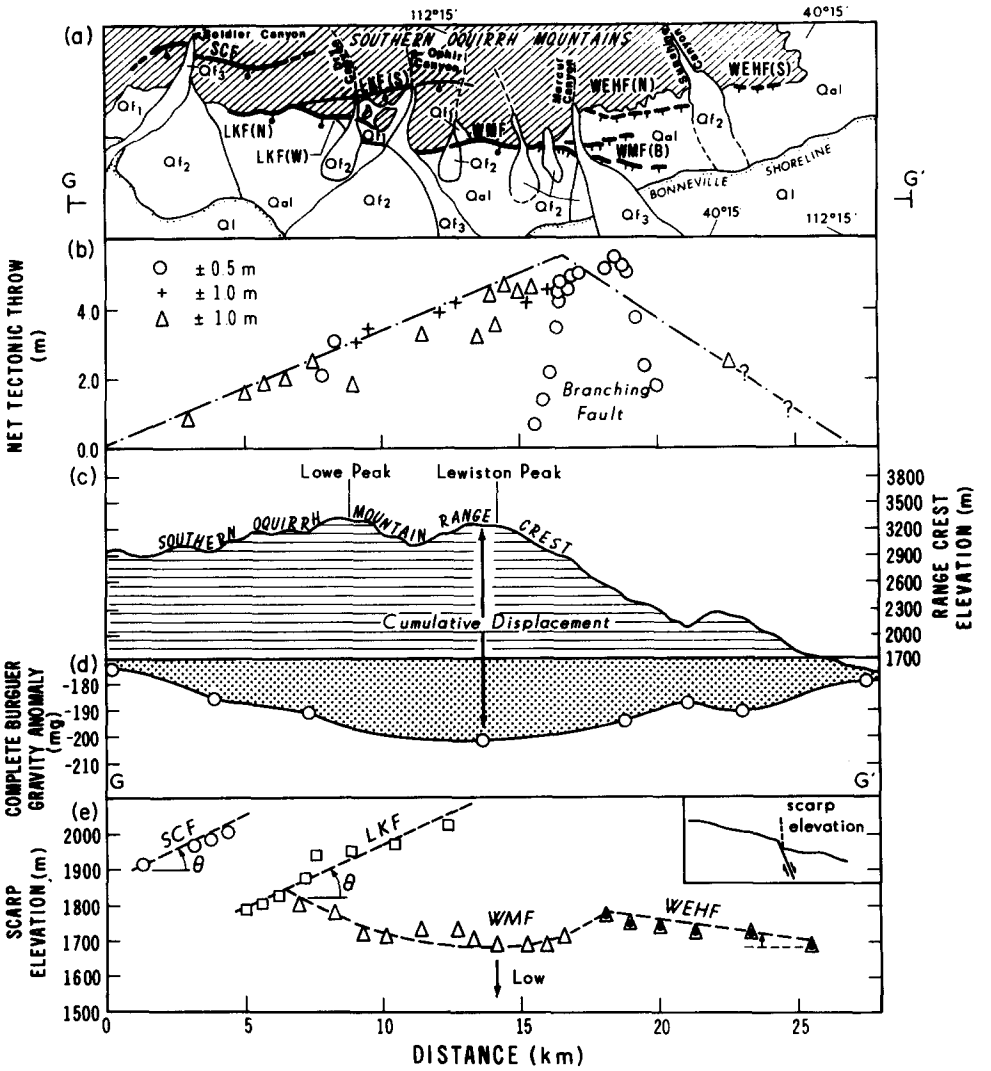

Fig. 2. Characteristics of the South Oquirrh Mountains fault zone. (a) A surficial geologic map of the South Oquirrh Mountains area. SCF = Soldier Canyon fault; LKF = Lakes of Killarney fault; (N)—northern section; (S)—southern section; (W)—western section; (B)—branch; WMF = West Mercur fault; WEHF = West Eagle Hill fault. Dotted line shows the Bonneville shoreline. Bold solid lines are the most recent fault scarps with bars in the hanging wall. Thin lines are abandoned fault traces. Q_{f1} = alluvial-fan unit 1 (pre-Bonneville Lake cycle). Pebble and cobble gravel in a matrix of sand, silt, and minor clay; moderately sorted. Q_{f2} = alluvial-fan unit 2 (early Bonneville Lake cycle). Pebble and cobble gravel in a matrix of sand, silt, and minor clay; moderately sorted. Q_{f3} = alluvial-fan unit 3 (late Bonneville Lake cycle). Pebble and cobble gravel, locally bouldery, in a matrix of sand, silt, and minor clay; poorly–moderately sorted. Deposited by perennial and intermittent streams, and debris flows. Q_{al} = undivided Quaternary alluvial deposits. Q_l = lacustrine deposits of Lake Bonneville. (b) Tectonic throw profile of the youngest fault scarps (younger than Q_{f2}). Circles are data from profiling across the youngest scarps in late Quaternary alluvium. Crosses are data measured on undetermined age scarps in both Quaternary alluvium and bedrock. Triangles are data measured on the youngest scarps in limestone bedrock with evidence of two events. (c) N–S elevation profile of the South Oquirrh Mountains range crest. Note that the elevation of the range crest continues to decrease northward by at least 4 km, outside the northern boundary of the frame. (d) Complete Bouguer gravity profile in the Rush Valley. Open circles are data points from complete Bouguer gravity map (1:500,000) of Cook *et al.* (1989). G–G′ is location of the profile (see Fig. 2a). (e) Fault scarp elevation profile. The cross-section in right-upper corner indicates the location of where scarp elevation is measured. θ is the along-strike rotation angle of secondary faults.

the fault according to Gilluly (1932), but Quaternary river terraces and alluvial fans at the mouths of Dry Canyon and Ophir Canyon are not faulted, implying that this fault branch has not been active in late Quaternary time.

The West Mercur fault is 8–9 km long and located about 2.5 km west of the Lakes of Killarney fault, in a right-stepping pattern (Fig. 2a). Between Ophir and Mercur canyons the fault strikes N30°–35° W and dips 55°–60°W. Quaternary alluvium in the hanging wall is faulted against Great Blue Limestone in the footwall. This contact forms a 20–25 m high fault scarp. The fault contact has been exhumed in the Daisy Gold Mine at several locations north of Mercur Canyon (Gilluly 1932). The West Mercur fault splits into two major fault branches near the mouth of Mercur Canyon (Fig. 2a). Quaternary fault scarps are located on both fault branches and extend at least 2 km south of the canyon, cutting through broad, gently-sloping alluvial fans.

The West Eagle Hill fault is located along the mountain front south of Mercur Canyon, where it extends for 8 km from Eagle Hill southward across Sunshine Canyon (Fig. 2a). This fault has not been previously mapped. The fault consists of two left-stepping sections.

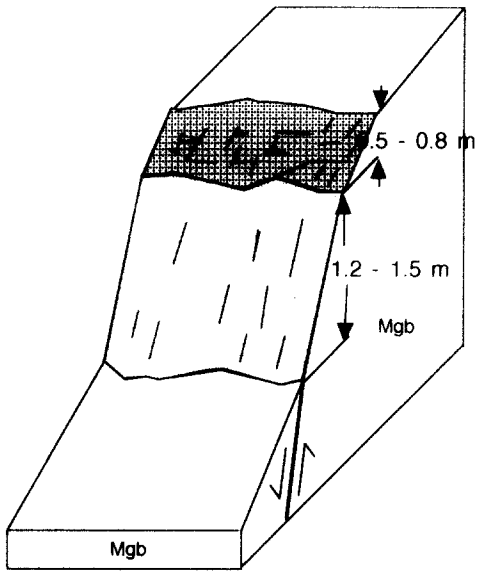

Fig. 3. Cartoon of a fault scarp in the northern section of the Lakes of Killarney fault. The fault scarp showing evidence of two rupture events and located 3 km north of Dry Canyon. M_{bg} = Great Blue limestone unit.

The northern section (WEHF(N)) is 4–5 km long and located 1 km to the east of the West Mercur fault, in a left-stepping sense. Late Quaternary alluvial deposits are cut by a fault scarp in the northern part of this fault section (Fig. 4), but the scarp is covered by younger alluvial fans farther south. The southern section (WEHF(S)) is 2–3 km long and located at the southern tip of the mountain range to the south of Sunshine Canyon, where Quaternary fans are cut by discontinuous scarps arranged in a left-stepping pattern.

HISTORY OF FAULTING IN LATE QUATERNARY TIME AND RUPTURE CHARACTERISTICS

History of Quaternary faulting

The surficial geology of Rush Valley is dominated by sediments deposited during the Bonneville Lake cycle between 28 and 12 ka (Gilbert 1890, Currey & Oviatt 1985, Currey 1990). Rush Valley was one of the Bonneville lake basins and has been an area of closed drainage since the beginning of normal faulting. Several lakes may have existed in the basin during the last 15 Ma (Hintze 1973, Hunt 1982). There are few surficial deposits older than the Bonneville Lake cycle, with the exception of early Quaternary alluvial deposits located on the foothills at elevations greater than 1580 m, the level of the highstand of Lake Bonneville.

The Bonneville shoreline, which marks the high stand of the lake and was formed about 15 ka, is preserved in Rush Valley at an elevation of 1580–1590 m. The height of the shoreline scarp cut in pre-existing surficial deposits varies from 10 to 15 m west of Soldier Canyon to a few meters west of Mercur Canyon. Alluvial fans located at different elevations along the mountain front developed during at least three significant pluvial events that changed the level of Lake Bonneville. Relative ages of the alluvial deposits may be differentiated based upon the degree of fan erosion, terrace incision and superposition of adjacent geomorphic surfaces. The oldest alluvial fans (Q_{f1}) are located along the foothills at elevations of 1960–1970 m (Fig. 2a). Sediments in these fans are semiconsolidated, consisting of pebble and cobble clasts in a matrix of sand, silt and minor clay, and are apparently older than the Lake Bonneville cycle based upon geomorphic and stratigraphic relations to the Bonneville shoreline. Some of these Q_{f1} deposits may be as old as 100–160 ka (?) if they correlate with similar surficial sedimentary deposits along the Wastach front as similar elevation (Scott *et al.* 1983, Machette 1984). Younger fans (Q_{f2}) are located in stream channels that are inset 20–50 m into the older fans, and spread out on the lower slopes of the mountains. These fans are the most widespread deposits in the area and may have formed during the early Bonneville lacustrine cycle. Stream terraces that are graded to each of the two older alluvial fan systems (Q_{f1} and Q_{f2}) are cut by the Bonneville shoreline which formed about 15 ka (Currey 1990). The youngest alluvial fans (Q_{f3}) developed since 15 ka, because they partly bury Bonneville shoreline deposits and are located at the mouths of ephemeral stream channels (Fig. 2a).

Fault scarps in the South Oquirrh Mountains fault zone cut Q_{f1} and Q_{f2} alluvial deposits (Fig. 2a), but not Q_{f3} deposits. Thus, the youngest surface faulting ocurred after deposition of the Q_{f2} fans and prior to the formation of the high stand of Lake Bonneville at about 15 ka. The fault scarp on the western branch of the West Mercur fault terminates at the Bonneville shoreline south of Mercur Canyon, where the fault scarp is partly eroded and buried as the result of wave action in Lake Bonneville (Everitt & Kaliser 1980). Between Dry and Ophir Canyons the fault scarps are 12–15 m high in Q_{f1} deposits, but only 4–5 m high in Q_{f2} deposits, indicating recurrent faulting.

The age of faulting inferred from the history of deposition and erosion along the western flank of the mountain range is also consistent with ages inferred from the morphology of fault scarps using the profiling method of Bucknam & Anderson (1979). Studies of fault scarps in the Great Basin suggest that the age of faulting may be inferred from an empirical relationship between maximum slope angle and scarp height (Bucknam & Anderson 1979, Pierce & Coleman 1986). The age of the scarp is estimated by plotting maximum slope angle against scarp height for measurements from several scarp profiles. The slope of the best-fit regression line is then used to infer age based on correlation with scarps of known age elsewhere within the Great Basin. The plotted lines of best fit for different-age fault scarps are parallel, but regression lines from younger scarps have a greater intercept than older ones (Machette 1989).

Profiles of late Quaternary scarps were measured in younger alluvial fan deposits (Q_{f2} along the western branch of the West Mercur fault (WMF(B)), the north-

Table 1. Morphologic characteristics of late Quaternary fault scarps in alluvium along the South Oquirrh Mountains normal fault zone

Profile station	Scarp height (m)	Net tectonic throw (m)	α_m* (°)	$\alpha_m - \alpha_f$ (°)	α_f† (°)
North section of West Eagle Hill fault					
P10	3.6 ± 0.8	1.6 ± 0.5	13.0 ± 2.0	6.5 ± 1.5	7.2 ± 1.5
P9	1.3 ± 0.5	0.8 ± 0.3	6.6 ± 1.5	4.0 ± 0.4	3.5 ± 1.0
P8	12.2 ± 2.0	5.1 ± 1.0	24.7 ± 3.0	15.5 ± 2.0	9.2 ± 1.5
P7	9.3 ± 1.5	4.1 ± 1.0	21.0 ± 3.0	11.5 ± 2.0	9.5 ± 1.5
P6	5.4 ± 1.0	2.5 ± 0.5	15.0 ± 2.0	8.2 ± 1.5	6.8 ± 1.0
P5	9.1 ± 1.5	4.1 ± 1.0	20.0 ± 3.0	12.5 ± 2.0	7.5 ± 1.3
P4	3.4 ± 0.8	1.9 ± 0.5	12.5 ± 2.0	6.5 ± 1.5	6.0 ± 1.0
P3	3.3 ± 0.8	1.5 ± 0.5	12.5 ± 2.0	7.0 ± 1.5	5.5 ± 1.0
P2	3.9 ± 0.8	1.7 ± 0.5	13.5 ± 2.0	6.0 ± 1.5	7.5 ± 1.5
P1	1.7 ± 0.5	0.9 ± 0.3	7.0 ± 1.5	4.0 ± 0.4	3.5 ± 1.0
North section of Lakes of Killarney fault					
P1	3.2 ± 0.8	2.1 ± 0.5	13.0 ± 2.0	9.0 ± 2.0	6.0 ± 1.0
P2	6.5 ± 1.0	3.6 ± 0.8	19.0 ± 3.0	12.0 ± 2.0	6.5 ± 1.0
Western branch of West Mercur fault					
P1	3.6 ± 0.8	2.5 ± 0.5	12.3 ± 2.0	8.8 ± 2.0	3.5 ± 1.0
P2	3.4 ± 0.5	2.2 ± 0.5	11.0 ± 2.0	9.5 ± 12.0	2.5 ± 1.0
P3	4.2 ± 0.8	3.1 ± 0.7	15.8 ± 2.5	12.0 ± 2.5	4.0 ± 1.0
P4	4.2 ± 0.8	3.1 ± 0.7	14.9 ± 2.5	11.0 ± 2.0	4.0 ± 1.0
P5-1	5.6 ± 1.5	4.6 ± 1.0	18.3 ± 3.0	15.0 ± 2.5	4.0 ± 1.0
P5-2	2.7 ± 0.5	1.8 ± 0.3	9.0 ± 1.5	7.0 ± 1.5	2.0 ± 1.0
P6	3.1 ± 0.7	2.1 ± 0.5	13.0 ± 2.5	9.0 ± 2.0	4.0 ± 1.0
P7	2.6 ± 0.5	0.9 ± 0.3	10.0 ± 2.0	3.5 ± 1.0	6.0 ± 1.5
P8	7.3 ± 1.5	5.2 ± 1.0	20.2 ± 3.0	15.0 ± 2.5	5.0 ± 1.5
P9	5.9 ± 1.0	4.3 ± 0.8	18.1 ± 3.0	13.0 ± 2.5	5.0 ± 1.5
P10	5.4 ± 1.0	4.5 ± 0.8	17.5 ± 2.5	15.0 ± 2.0	3.0 ± 1.0
P11	5.6 ± 1.0	4.4 ± 0.8	17.8 ± 2.5	14.0 ± 2.0	3.0 ± 1.0
P12	5.9 ± 1.0	4.7 ± 0.8	18.0 ± 2.5	14.5 ± 2.0	3.5 ± 1.0

*α_m = maximum scarp slope angle.
†α_f = angle of far slope.

ern section of the West Eagle Hill fault (WEHF(N)), and in the western branch of the Lakes of Killarney fault (LKF(W)) (Table 1; Figs. 2a, 4 and 5). Regression lines relating scarp height to the maximum slope angle indicate that the scarps may be only slightly older than 15 ka, the age of the Bonneville shoreline (Fig. 6). Barnhard & Dodge (1988) reached a similar conclusion based on 11 profiles along the western branch of the West Mercur fault. Our data indicate that the Quaternary scarps along the Lakes of Killarney, West Eagle Hill and West Mercur faults are similar in age because the data points from the three faults are located roughly along the same

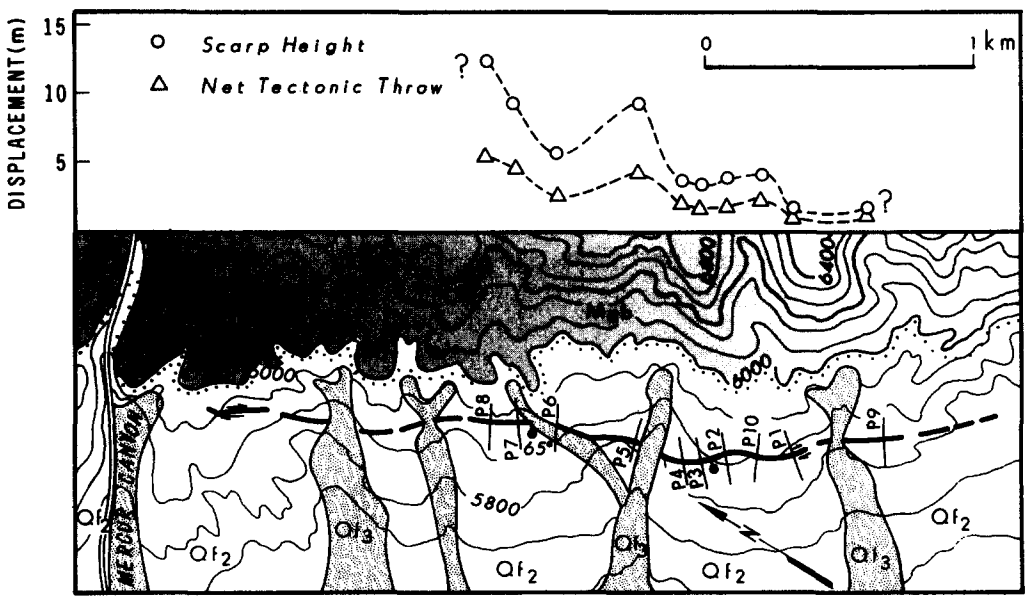

Fig. 4. Late Quaternary fault scarp and displacement characteristics along northern section of the West Eagle Hill fault. Short lines mark profile locations (see Table 1). Dotted line indicates the contact between alluvium and bedrock. M_{bg} = Great Blue Limestone. Q_{f2} = alluvial deposits of early Bonneville age. Q_{f3} = alluvial deposits of late Bonneville age.

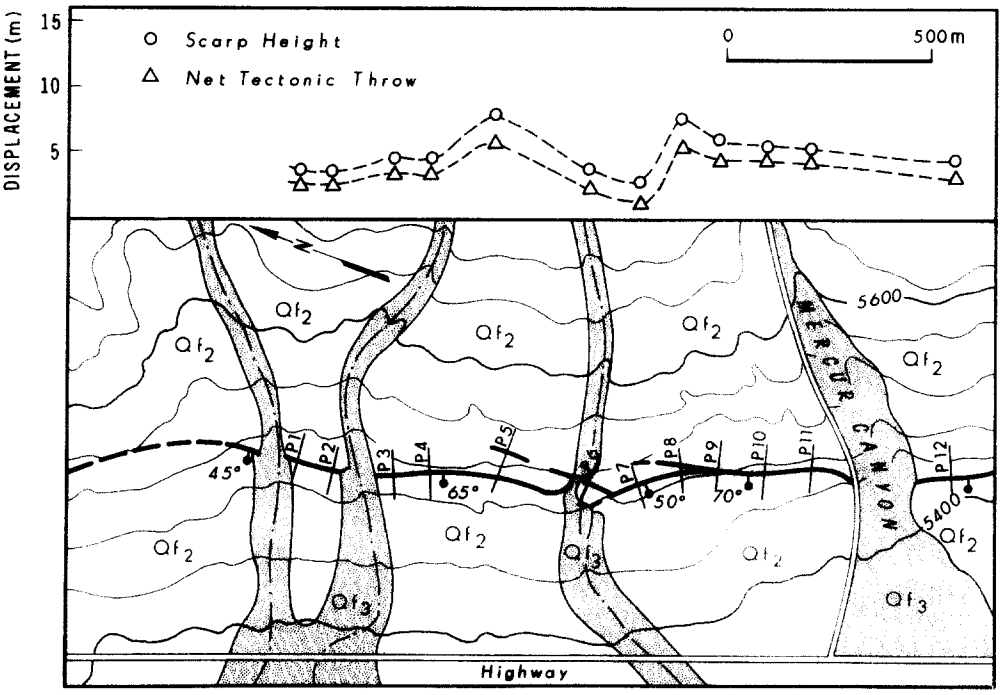

Fig. 5. Late Quaternary fault scarp and displacement characteristics along west branch of the West Mercur fault. See Fig. 4 for symbol explanation.

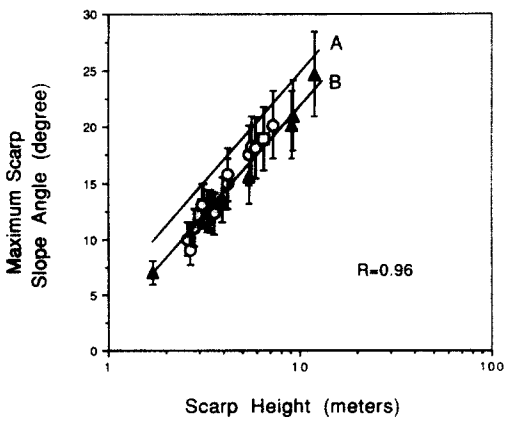

Fig. 6. Lines of best fit for morphometric data from the Bonneville shoreline (A) and the South Oquirrh Mountains normal faults (B). The regression line of the Bonneville shoreline from Bucknam & Anderson (1979). R = correlation coefficient. Triangles are data from WEHF(N). Circles are data from WMF(B). Boxes data from LKF(B). See Fig. 2(a) for locations.

regression line (Fig. 6). However, the temporal resolution of the dating method when multiple-event scarps are used in the analysis, would not allow age differences of a few thousand years to be distinguished.

Rupture characteristics

Information on tectonic displacement was collected along the four individual faults of the SOMFZ by profiling fault scarps produced during the last one or two earthquakes. We focused on three types of fault scarps that are developed along the mountain front: bedrock scarps, alluvial-fan scarps and alluvium-bedrock scarps (Fig. 2b). The alluvial-fan scarps are developed in Q_{f2} fan deposits; most are located south of Mercur Canyon, but a few are north of Ophir Canyon (Fig. 2a). The alluvium-bedrock scarps are mostly located between Mercur and Ophir canyons where the bedrock is faulted against Quaternary alluvial fan deposits. Bedrock scarps are located north of the Dry Canyon where the scarps lie 10–20 m above the contact between bedrock and alluvium.

The tectonic throw of the youngest fault scarps varies along strike, attaining greatest values in the central part the fault zone between Ophir and Mercur canyons, and decreasing in magnitude toward each end of the fault zone (Fig. 2b). The region of low surface offset in the center of the fault zone may be due to fault branching to accommodate the displacement along the overlapping faults, rather than a true, local minimum in displacement. Most of the scarps were developed during two or more paleo-earthquakes, based on known scaling relationships between fault length and displacement, and the morphology of the scarps. The total length of the normal fault zone is about 25 km. The maximum tectonic displacement at the surface during an earthquake of magnitude 7 for a fault zone of this length is estimated to be approximately 3 m in the Basin and Range Province based on statistical relationships between fault length and the maximum surface offset of historic earthquakes compiled by Slemmons (1977), Bonilla *et al.* (1984) and Mason (1992). Scarps in Quaternary alluvial fans in the western branch of the Lakes of Killarney fault are 11–15 m high, and presumably developed during at least three, and probably four or more, earthquakes. Tectonic displacement across scarps in younger alluvial deposits (Q_{f2}) at the mouth of Mercur Canyon in the West Mercur fault is 4–5 m, and probably developed during at least two earthquakes. The maximum displacement of 4–5 m measured across scarps in the West Eagle Hill fault sections is also consistent with development

during at least two earthquakes. Differential weathering on the limestone fault scarps at the northern section of the Lakes of Killarney fault indicates two surface faulting events, the younger with a displacement of 1.2–1.5 m and the older with a minimum displacement of 0.5–0.8 m (Fig. 3).

Spatial correlation between fault geometry and displacements

There is a general correlation between fault geometry (Fig. 2a), along-strike variation in surface offsets measured across late Quaternary scarps (Fig. 2b), elevation changes along the Oquirrh Mountains range crest (Fig. 2c) and accumulation of late Tertiary and Quaternary sedimentary rocks beneath Rush Valley as inferred from complete Bouguer gravity data (Fig. 2d). The maximum surface offset, measured from four main individual faults, is 2 km south of the Mercur Canyon, but when adding surface offsets of the branching faults to the fault zone the maximum offset appears to be located at the southern part of the West Mercur fault, close to the apex of the convex-shaped fault zone. The range crest elevation and complete Bouguer gravity anomaly profiles have a similar characteristics to the scarp displacement profile, in that the maximum range crest elevation and minimum Bouguer gravity anomaly occur opposite the central part of the fault zone, where late Quaternary surface offset is greatest. All three profiles taper off towards both ends of the fault zone. These correlations suggest that the total displacement across the fault zone varies laterally in a similar manner to that measured across late Quaternary scarps. This type of correlation has also been documented in some historic earthquake and late Quaternary scarps in the Basin & Range province, such as the 1983 Borah Peak earthquake rupture in Idaho (Crone *et al.* 1987) and the Wasatch fault zone in Utah (Nelson & Personius 1990). In other words, the net displacement accumulated over periods of millions of years is greatest in the central part of the fault zone and tapers off towards the ends, which may imply that the characteristics or displacement pattern of the rupture process has persisted over several millions of years.

Elevations of fault scarps vary systematically along the strike of the South Oquirrh Mountains fault zone (Fig. 2e). Such elevation differences may provide information on characteristics of tectonic displacement over a time scale of several million years (Wu 1993). Scarp elevations increase from north to south along the Soldier Canyon and Lakes of Killarney faults. However, scarp elevations gently decrease towards the south to obtain the lowest elevations in the West Mercur fault, then increase to a high point at the northern end of the West Eagle Hill fault and systematically decrease southward (Fig. 2e). Noticeably, the lowest elevation scarps broadly coincide with the maximum displacements measured across late Quaternary scarps (Fig. 2b), the maximum elevation of the range crest (Fig. 2c) and the deepest part of the sedimentary basin beneath Rush Valley as inferred from the complete Bouguer gravity data (Fig. 2d). These correlations suggest that the individual faults formed at both north and south of the West Mercur fault have been rotated northward and southward, respectively, with respect to horizontal axis perpendicular to the fault strike and located at central part of WMF. The rotation was caused by the uplift of the footwall of WMF which has larger cumulative displacement than the adjacent faults. Footwall displacements of the West Mercur fault would uplift both the hanging wall and footwall of the adjacent individual faults (LKF in the north and WEHK in the south) because they are partly located in the footwall block of WMF. The rotation of these adjacent faults is also affected by along-strike variability in the footwall deformation of the West Mercur fault, which is larger at the center of the fault and smaller at its ends.

Decreasing length of individual faults (SCF, LKF, WMF, WEHF(N) and WEHF(S)) towards both the south and north ends of fault zone may also imply that the largest displacement is located at the central part of the fault zone because the length of faults is proportional to the maximum cumulative displacement according to Watterson (1986) and Walsh and Watterson (1988, 1989). For example, the West Mercur fault is 10 km long in the central part of the fault zone, the Lakes of Killarney fault is 8 km long to the north, and the Soldier Canyon fault is only 5 km long to the further north; the same situation applies to the south part of the fault zone (Fig. 2a).

GEOMETRIC AND KINEMATIC CHARACTERISTICS

Fault planes near the surface have been exhumed by mining, faulting and erosion at several places along the South Oquirrh Mountains fault zone. Orientations of fault surfaces and striations were measured at 14 locations on the Soldier Canyon, Lakes of Killarney, West Mercur and West Eagle Hill faults (Fig. 7). We made between two and 15 measurements of fault plane orientations and striation directions at each location. Fault surfaces group about two dominant orientations: one group strikes N10°W ± 10° and dips 65° ± 10°W, and the other strikes N43°W ± 10°, dipping 68° ± 10°W (Fig. 8). Orientations of striae on the fault surfaces vary significantly from place to place, but slip directions concentrate about an average trend of S70°W (Fig. 8b). Some fault surface exposures contained two or even three sets of differently oriented striations separated by 15–20° in rake, but careful inspection of the striae for evidence of relative time of formation produced no consistent results. The following geometrical properties of the fault surfaces and striae are evident (Fig. 8b): (1) poles to fault surfaces form two maxima separated by approximately 33° ± 3°; and (2) the striae plunge to the west-southwest, close to the line defined by the intersection of the two fault planes associated with the fault pole maxima in the diagram.

The angle of 33° between the two fault pole maxima

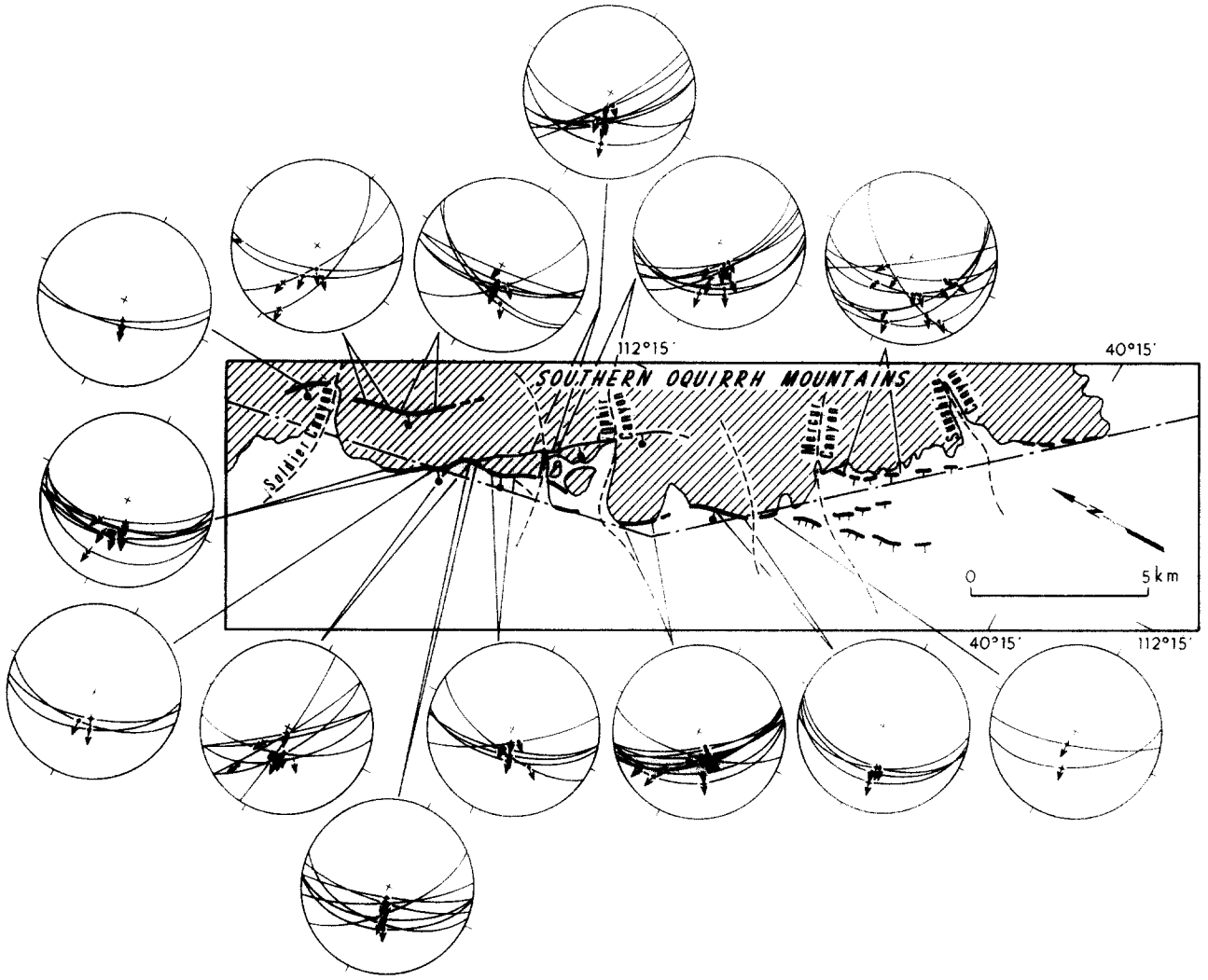

Fig. 7. Location map of fault exposures and stereonet plots of fault plane orientations (great circles) and striations (arrows). Plots are lower-hemisphere projection.

(Figs. 8b and 9a) is determined for 'meter-scale' surfaces on rock outcrops, but in fact, the angular separation between dominant fault strikes appears to be relatively constant regardless of the scale of measurement (Table 2). That is, subsurface map data at a scale of 5–100 m from exposures of the West Mercur fault in the Daisy Mine (Fig. 9b) and mapped fault traces of 1.5–10 km (Fig. 9c) both form two maxima in rose diagrams, separated by approximately 32–35° in trend.

The information on variability in fault strike at different scales, together with inspection of surface exposures and the map of fault exposures in the Daisy Mine all indicate that fault surfaces are corrugated, and that these corrugations are non-cylindrical (Fig. 10). For example, miners produced gold ore directly out of the West Mercur fault in the Daisy Mine, so that the mine map provides direct evidence for the geometry of the fault surface in both horizontal and vertical section (Fig. 10). The following geometrical features are beautifully displayed on the mine map: (1) ridges and furrows in the corrugated fault surface change amplitude and some of them apparently disappear over vertical distances of a few tens of meters; (2) the average slip direction on the West Mercur fault is subparallel to the long axes of the corrugations; and (3) the intersection of the fault with the earth's surface should generate a sinusoidal fault trace that is convex towards the hanging wall at positions of structural ridges, and concave towards the hanging wall at positions of structural troughs. The general sinusoidal or convex- and concave-shaped fault traces within the South Oquirrh Mountains fault zone, together with our other orientation data, indicate that corrugated fault geometry like that found in the Daisy Mine is present as scales from less than 1 m to tens of kilometers (Fig. 11).

DISCUSSION

Our study of the South Oquirrh Mountains fault zone motivates us to propose a model for the growth and development of the fault zone that is consistent with the observed fault geometry and displacement field. We then speculate further on the structural relationships of the three major fault zones along the western flanks of the Oquirrh and East Tintic mountains.

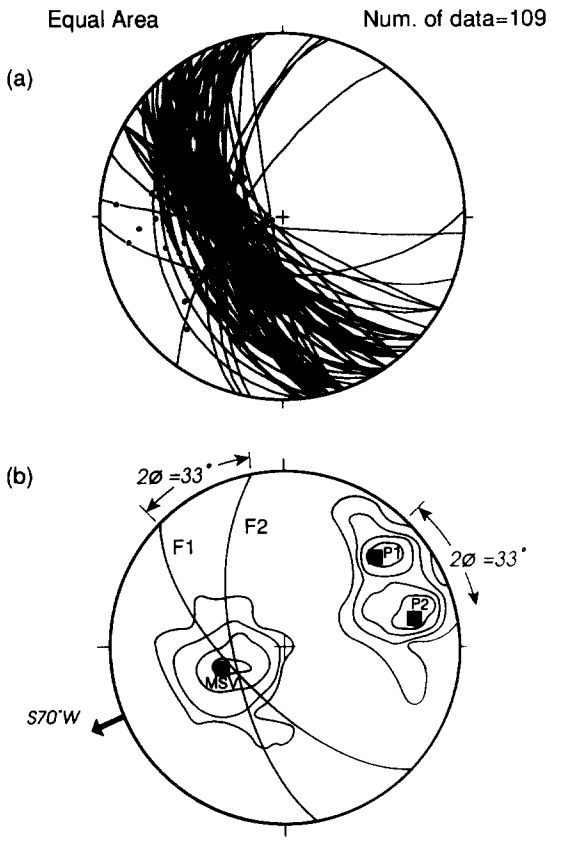

Fig. 8. Equal-area stereographic projection showing geometric and kinematic characteristics of the South Oquirrh Mountains normal faults. (a) Total fault plane and slip vector orientations from 14 locations shown in Fig. 7. (b) Pole contours showing concentrations of poles of fault planes and slip vector orientations. P1 and P2 are poles of two dominant orientations (F1 and F2) of measured fault planes. MSV = mean orientation of slip vectors. 2ϕ = geometric angle between two groups of fault surfaces.

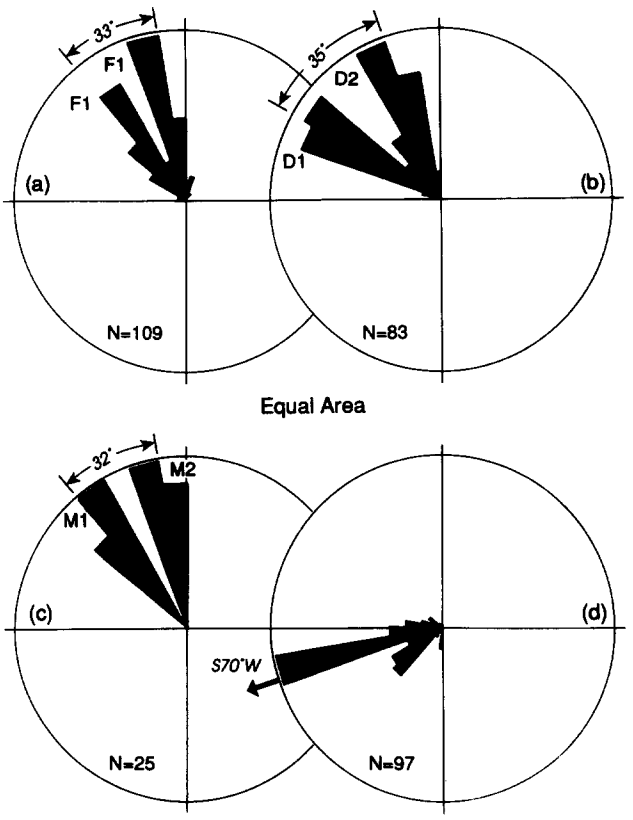

Fig. 9. Rose diagrams showing two dominant orientations and dominant slip direction on fault surfaces of different scales. (a) Measured on outcrops (see Fig. 8). (b) Measured on meter-scale fault map of Daisy mine (see Fig. 10). (c) Measured on km-scale fault map (see Figs. 2a and 11). (d) Mean slip direction. N = number of data collected.

Self-similar properties of fault surfaces

Fault surface topography may be modeled as a fractional Brownian profile in which the variance in topography (Δv^2) scales with along-strike distance or spatial wavelength (Δx) by the following rule (Mandelbrot 1983, Barnsley *et al.* 1988, Power & Tullis 1991):

$$\Delta v^2 = k\Delta x^{2H}, \quad (1)$$

where k is a constant, and H is the Hurst exponent which is related to fractal dimension (D) by the equation $H = 2 - D$ for a two-dimensional profile. The square root of equation (1) provides a formula for the average change in angle of a surface between two points separated by distance (Δx).

$$\tan(\phi/2) = \Delta v/\Delta x = k^{0.5}\,\Delta x^{(H-1)}. \quad (2)$$

If $D = 1.0$, $H = 1.0$ and $\tan(\phi/2) = k^{0.5}$ or ≈ 0.29, given the angular measurements of fault orientation in the South Oquirrh Mountains fault zone in which the angular dispersion between fault surfaces measured at scales from 1 m to several kilometers is nearly constant ($\phi = 32° \pm 5°$). We have also studied other normal faults in the Basin and Range province and revealed that there is a linear relation between the wavelength and amplitude or ridges or furrows on the corrugated fault surface (Wu 1993). These imply self-similar scaling of fault surface topography measured crudely in an along-strike direction, different from the situation for self-affine scaling of fault surface topography in which $H-1$ is not zero (i.e. $D \neq 1.0$). If $D = 1.2$, so that $H = 0.8$, then $\tan(\phi/2)$ is not a constant, but depends on $\Delta x^{(-0.2)}$, a non-linear function of profile length. In this cse, the angle (ϕ) decreases as a function of increasing distance (Δx), which is not consistent with our observations. We conclude that within the resolution of our measurements the angular measurements of fault strike at various lengths indicate a self-similar fault surface topography or profile geometry.

Development of the South Oquirrh Mountains fault zone

A model for the evolution of the South Oquirrh Mountains fault zone must incorporate the following features. (1) The trace of the fault zone is convex towards the hanging wall in map view, with the apex located near the center of the fault zone at the point of greatest displacement. (2) There is a systematic change in the sense of step-over between faults comprising the fault zone. Faults located in the northern half of the zone are arranged in a right-stepping en échelon pattern, but are left-stepping in the southern part of the fault zone. (3) There is a systematic change in the elevation of fault scarps. Fault scarp elevations are lowest at the center of

Table 2. Fault geometry and kinematic characteristics of the South Oquirrh Mountains fault zone

Scales of faults	Dominant orientations	SDV*	Geometric angle	MSV† trend	Number of data	Locations
0–2 m	F1,N43°W; F2,N10°W	±07°	2ϕ=33°±5°	S70°±10°W	N = 109	14 sites (Fig.7)
5–100 m	D1,N55°W; D2,N20°W	±10°	2ϕ=35°±8°	S68°±10°W	N = 83	Daisy mine (Fig.10)
1.5–25 km	M1,N43°W; M2,N10°W	±09°	2ϕ=32°±5°	No data	N = 25	Fault system (Fig.11)

*SDV=standard deviation; †MSV=mean slip direction. See Fig. 9 for details.

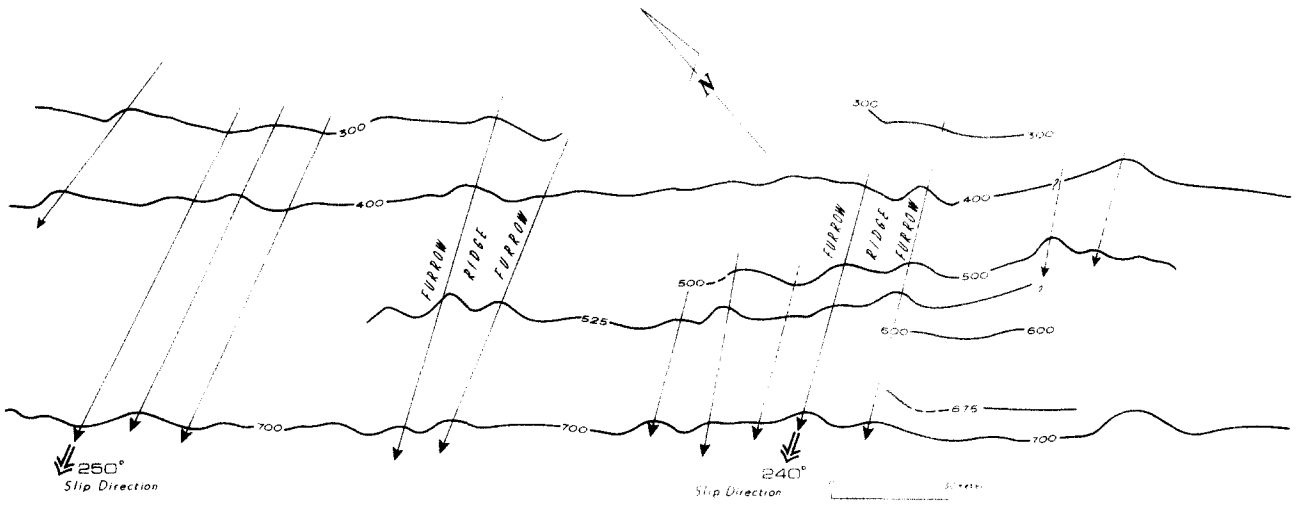

Fig. 10. Contour map showing the fault surface topography of West Mercur fault at Daisy mine (see Fig. 11 for map location). Contours indicate the depth of the fault surface in feet. Arrows indicate slip orientations inferred from ridge and furrow structures in the fault surface. Base map was provided by Barrick Gold mine.

the fault zone, rise towards the intersection between individual faults, and then decrease systematically towards the end of each fault. (4) The ends of the Lakes of Killarney, Soldier Canyon and West Eagle Hill faults are apparently inactive in those areas where they overlap with one another or with the West Mercur fault. (5) The lengths of individual faults decreases away from the central part of the fault zone. These properties appear to be common to other normal fault zones (Wu 1993),

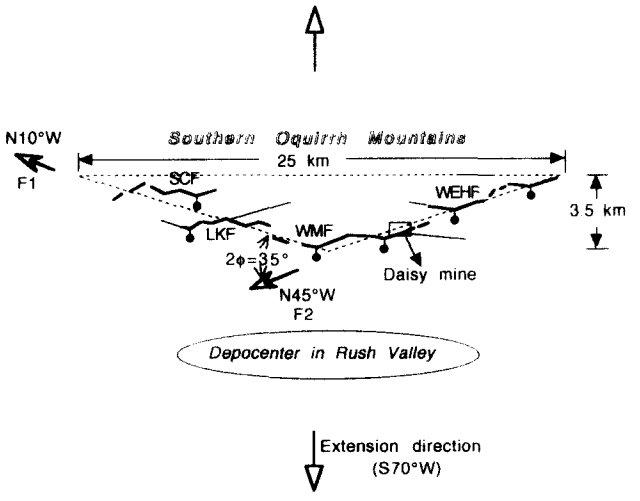

Fig. 11. Geometric pattern of the South Oquirrh Mountains fault zone showing self-similar characteristics of fault geometry of different orders. F1 and F2 indicate two main fault orientations, which are dominant in the fault zone as a whole and also in each individual fault (SCF, LKF, WMF and WEHF). Boxed area is the location of the Daisy mine.

suggesting that a model for the evolution of the South Oquirrh Mountains fault zone may apply elsewhere.

The model we propose here is related to asymmetry of displacements in the hanging wall and footwall. In this qualitative model, the fault zone initiates at a point and then grows bilaterally. Strains, and therefore the orientations of new faults, is strongly influenced by differential displacements between the hanging wall and footwall. The displacement fields in the hanging wall and footwall of a normal fault are neither symmetrical nor equal in magnitude to one another (Savage & Hastie 1966, Masiha & Smylie 1971, Gibson *et al.* 1989). Growth of a normal fault is accompanied by increasing displacement and lateral propagation of the fault tips along strike (Fig. 12). The local strain field is dominated by down-bowing of the hanging wall and a lesser amount of upward-bowing of the footwall (Fig. 12b). The net effect is to superimpose a local shear strain component, caused by the asymmetric displacements between the hanging wall and footwall and parallel to fault strike, on the regional and fault-perpendicular extensional strain. This rotates the strain field in front of the advancing fault. If the fault grows bilaterally, then new faults produced in front of the two fault tips may preferentially develop in an en échelon pattern, with an opposite sense of offset at the two ends of the primary fault (Fig. 12b). That is, there will be opposite senses of lateral shearing at each tip, causing faults to form in a right-stepping pattern under the sinistral shear component at one end, and a left-stepping pattern under dextral shear at the other end. Newly-formed secondary faults therefore

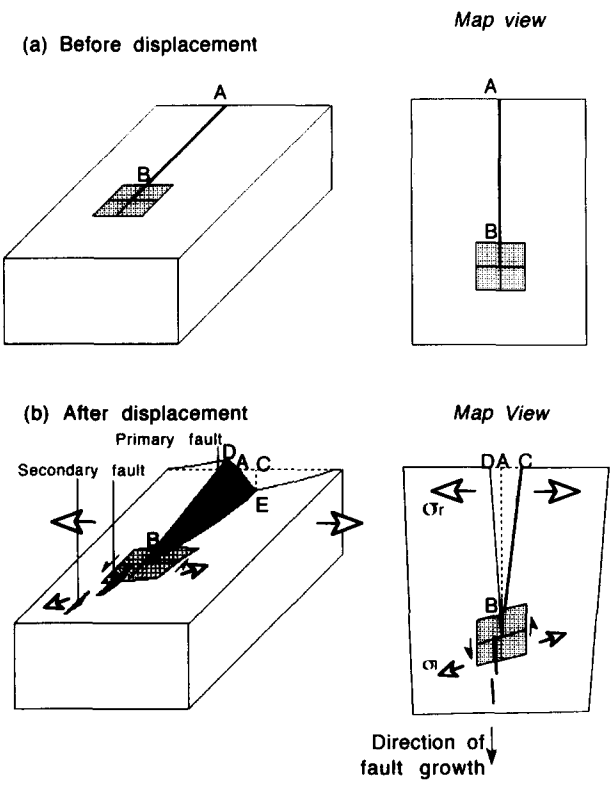

Fig. 12. Speculative model of normal fault growth associated with asymmetric displacements. (a) Normal fault before displacement. A–B indicates the fault trace in half-space. (b) Growth of the normal fault after displacement, and its deformation pattern. D–A = displacement contributed by uplift of the footwall. C–E = displacement contributed by subsidence of the hanging wall. D–C indicates maximum value of extension.

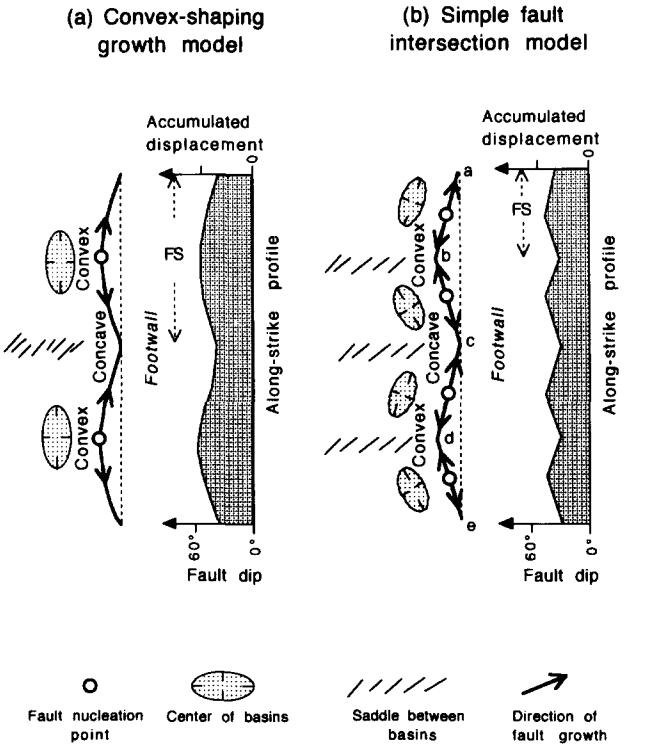

Fig. 13. Models of fault growth associated with crustal deformation. (a) Proposed model showing formation of fault geometry by growth of faults from convex initiation points to concave linkage points. (b) Simple fault intersection model showing fault geometry formed by intersections of planar fault surfaces. FS = length of fault section.

step into the footwall block, making the trace of the fault zone convex in map view. When two along-strike fault zones grow in this manner and link together, the intersection point is marked by a cuspate or concave-shaped fault trace. Because it is the youngest fault section, the concave-shaped fault section has less cumulative displacement than exists in the convex-shaped fault section where the fault zone is nucleated (Fig. 13a).

We also note that the ends of overlapping faults become abandoned in the footwall as deformation progresses and the faults link together. The abandoned parts of the Lakes of Killarney and West Eagle Hill faults in the area where they overlap the West Mercur fault are an example (Figs. 2a & e). This bilateral fault growth model is also consistent with the observed spatial pattern and elevation changes of fault scarps along the Lakes of Killarney, Soldier Canyon and West Eagle Hill faults. If the West Mercur fault formed first, and then grew bilaterally, the footwall should be progressively tilted or flexed eastward, with maximum tilt in the central part of the fault zone and decreasing tilt toward the ends. Younger en échelon faults (LKF and SCF in the north, and WEHF in the south) formed immediately to the east of the tips of the growing fault zone must then be partly uplifted within the footwall block of the older West Mercur fault, attaining greater elevation on the mountain sides (Fig. 2e).

The *bilateral fault growth model* proposed here generates a convex-shaped fault zone in map view (Fig. 13a). This model has important implications for interpreting the geometry and deformation patterns of normal faults, particularly in zones several tens of kilometers in length. The *fault intersection model* provides an alternative interpretation of sinuous or scalloped fault traces (Fig. 13b). This model has been used to interpret normal fault geometry (Reches, 1983, Reches & Dieterich 1983), Susong *et al.* 1990) and predicts very different relationships between fault geometry and crustal deformation than the growth model proposed here. In the fault intersection model, the sinuous or scalloped fault trace reflects intersections or independently initiated and differently oriented fault segments. Apex points (a,b,c,d and e in Fig. 13b) in the sinusoidal fault trace are formed where the intersection line between two adjacent fault segments intersects the Earth's surface. If this model is correct, the apex points should be the sites where vertical displacement is less than the intervening fault sections. This is because the intersection line between two faults always plunges at a smaller angle than the dip of the faults, resulting in smaller vertical displacements in those areas. Furthermore, the intersection areas between fault segments are assumed to be the locations where two individual fault segments link together during lateral fault growth. Thus, they are located away from the nucleation points and accumulate less deformation because the displacement of normal faults is maximum at the nucleation area and decreases in the propagation direction (Walsh & Watterson 1988, 1989). Consequently, points of maximum subsidence in the hanging

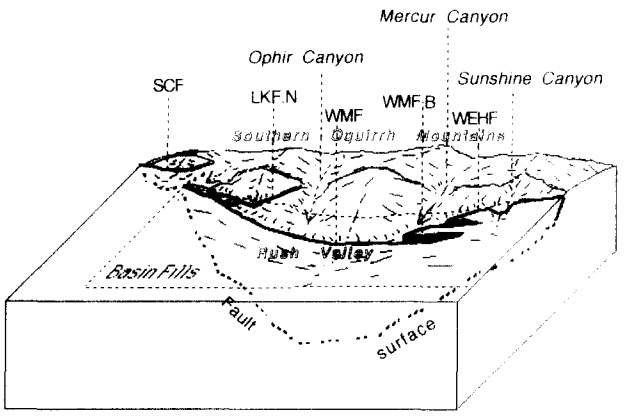

Fig. 14. Three-dimensional view of the South Oquirrh Mountains showing geomorphological characteristics of normal faults.

wall and maximum uplift in the footwall are predicted to occur on either side of the apices in the fault trace, whereas the minimum displacements coincide with the apex points (Fig. 13b). This is a fundamentally different relationship than predicted by the bilateral growth model. Moreover, the fault intersection model does not predict a systematic en échelon pattern between faults as the proposed growth model does (Figs. 12, 13 and 14).

The relationship between fault geometry and deformation pattern in the South Oquirrh Mountains fault zone is most consistent with the proposed fault growth model. Based on this model, we propose the following steps for the evolutionary history of the South Oquirrh Mountains fault zone (Fig. 15). (1) The West Mercur fault initiated and began to grow laterally (time a). (2) Local strain rotation at the northern end of the West Mercur fault caused a right-stepping en échelon offset and formation of the younger Lakes of Killarney fault; similar growth and local stress rotation at the southern end of the West Mercur fault formed the West Eagle Hill fault (time b). (3) The Soldier Canyon fault was formed immediately north of the Lakes of Killarney fault as the Lakes of Killarney and West Mercur faults became linked together, and the fault zone continued to grow towards the north (time c). Linking of the Lakes of Killarney and West Mercur faults caused the southern section (LKF(S)) of the Lakes of Killarney fault to become inactive. (4) The western branch of the West Mercur fault was produced by a local perturbation in displacement of the main fault zone (time d), the origin of this perturbation is not known. Apparently, this branching fault did not make much contribution to the total uplift of the mountain block.

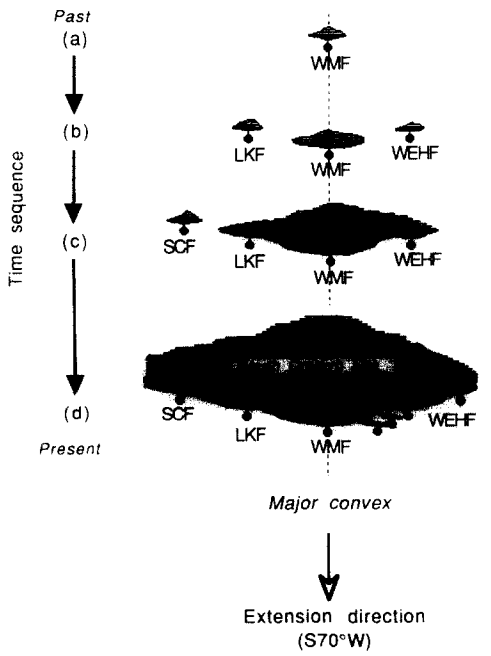

Fig. 15. Speculative growth model of the South Oquirrh Mountains fault zone. Shaded areas are the uplift of the footwall block. See text for the full name of WMF, WEHF, LKF and SCF.

The bilateral fault growth model predicts along-strike variations in mountain range topography and an integrated history of displacement that are similar to those proposed by Cowie & Scholz (1992), although their model does not consider a specific pattern of fault growth. However, the model requires further development and testing by numerical modeling and studies of other fault zones. The general geometry and displacement features predicted by the model are common to parts of other fault zones within the Basin and Range and Rocky Mountain region of the western United States, but there are also exceptions that are not predicted by the bilateral growth model (Bruhn 1992).

Relationship between the South Oquirrh Mountains fault zone and adjacent fault zones

In map view, fault traces appear to contain deflections or 'sinusoids' of variable wavelength and magnitude that are superimposed on one another (Fig. 11). This geometry presumably originates by growth and linking together of faults of variable sizes, and reflects a hierarchy in dimensional scaling, with larger faults formed by ensembles of smaller ones (King 1986, Wu 1993). This process may explain the consistent angular dispersion and corrugation of fault surfaces observed at the meter scale in outcrops (Figs. 8 and 9a), the 10 m scale in the Daisy mine (Fig. 9b) and the 1–20 km scale in the map of the South Oquirrh Mountain fault zone (Figs. 9c and 11). The linking of fault sections of different scales, from millimeters to tens of kilometers, may follow the fault growth mechanism proposed in the previous discussion (Figs. 12, 13 and 15). Here, we consider linking of the West Mercur fault to the Lakes of Killarney fault and the West Eagle Hill faults to be lower-order linking between smaller faults, whereas linking of the South Oquirrh Mountains fault zone to the adjacent North Oquirrh Mountains and East Tintic Mountains fault zones is considered to be higher-order linking between larger faults (Fig. 16).

The normal fault system along the Oquirrh Mountains and East Tintic Mountains consists of three separate fault zones, each convex towards the hanging wall in map view (Fig. 16b). This observation, together with the arguments concerning the growth history of the South

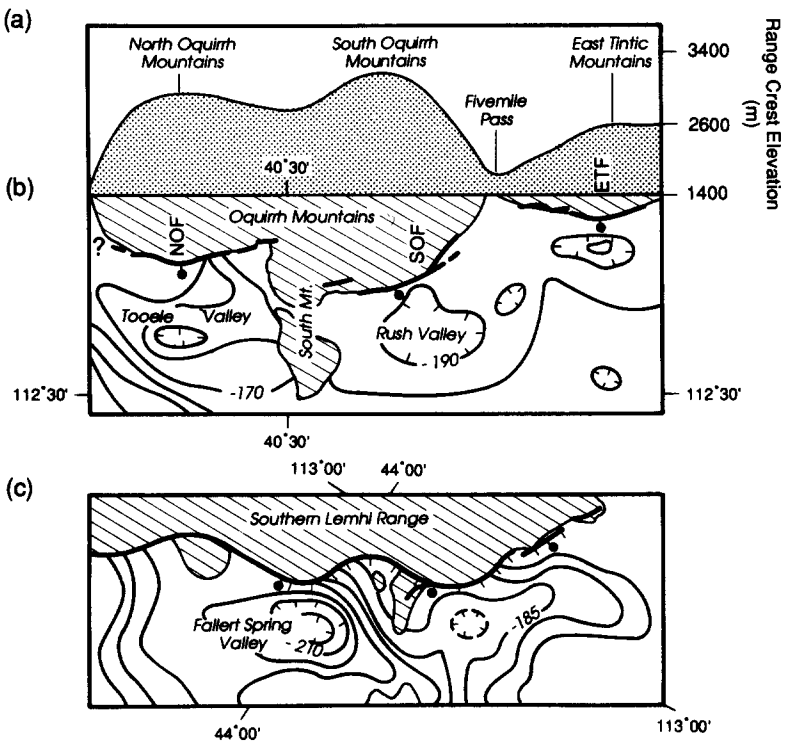

Fig. 16. Comparison between fault structures of Oquirrh–East Tintic Mountains normal fault zones and the southern Lemhi Range normal fault zone. (a) Elevation profile along the Oquirrh–East Tintic Mountains range crest. (b) Normal faults along the western flank of the Oquirrh and East Tintic Mountains and complete Bouguer gravity contours in the adjacent basin valleys (Cook *et al.* 1989), showing unlinked normal fault zones. SOF = South Oquirrh Mountains fault zone. NOF = the North Oquirrh Mountains fault zone. ETF = the East Tintic Mountains fault zone. (c) Normal fault zone along the southwestern flank of the southern Lemhi Range and complete gravity contours (Bankey *et al.* 1985), showing the geometry of linked normal faults. Teeth marks are the late Quaternary fault scarps.

Oquirrh Mountains fault zone discussed above, suggests that each fault zone developed independently, and grew towards one another over time. This speculation is supported by the distribution of late Tertiary sedimentary rocks in the adjacent basins. Positions of maximum sedimentary thickness inferred from gravity data occur next to the apex of each convex-shaped fault zone, and the range crest elevations of the Oquirrh and East Tintic Mountains obtain maxima in the central part of each fault zone and minima adjacent to the ends of each fault zone (Fig. 16a). However, these three normal fault zones are not yet fully linked. They are separated by two structural boundaries: South Mountain in the north and Fivemile Pass in the south.

South Mountain marks the structural boundary separating the North and South Oquirrh Mountains fault zones and may also be a fundamental earthquake rupture boundary, because the history of Quaternary surface faulting is different on either side of this boundary (Everitt & Kaliser 1980, Barnhard 1988, Barnhard & Dodge 1988, Olig *et al.* 1993). The last earthquake rupture in the North Oquirrh Mountain fault zone occurred about 7000 years B.P. based on trench data of Olig *et al.* (1993). There is no evidence for a major fault that cuts across this boundary, although Gilluly (1932) mapped a normal fault in the bedrock within the eastern part of the boundary. This fault apparently dies out in the southern part of the boundary rather than cutting completely through it.

The nature of the fault boundary near Fivemile Pass is more speculative because it is not exposed. Evidence of a boundary at this location includes low range crest elevation (Fig. 16a) and a buried bedrock ridge separating the basins beneath Rush Valley and West Tintic Valley as inferred from the Bouguer gravity data (Fig. 16b). No Quaternary scarps were observed near the Fivemile Pass area. However, an 8 km long late Quaternary scarp is present at the northern tip of the East Tintic Mountains. The age of the scarp is controversial. Everitt & Kaliser (1980) suggested a post-Bonneville age for the scarp based on the cross-cutting relationship between the fault scarp and alluvial fans, but nine scarp profiles collected by Barnhard & Dodge (1988) indicate that the scarp may be older than the Bonneville shoreline.

Characteristics of the fault geometry, structures, displacement fields and landforms in the Oquirrh and East Tintic Mountains fault zones have been also observed in other normal fault zones in the Basin and Range province in the western United States, implying that the fault growth model proposed in this study may apply elsewhere (Wu 1993). Figure 16(c) shows the structural characteristics of the southern Lemhi Range fault zone in Idaho. In this fault zone, the major convex-shaped fault sections have a wavelength of 23 ± 2 km, and correlate with the complete Bouguer gravity lows in the adjacent basin valleys as well as the maximum surface offset measured across late Quaternary fault scarps (Wu 1993, Bruhn *et al.* unpublished report). The largest

concave-shaped sections may be the locations where the different faults linked together and coincide with gravity saddles and bedrock salients in the hanging wall, where displacement is presumably smaller. Notably, the southern Lemhi Range fault zone is structurally similar to the Oquirrh Mountains fault system, particularly in the correlation between fault geometry and deformation pattern. The main difference between the two fault systems is that the 23 km long higher-order fault segments have linked together along the southern Lemhi Range fault zone, but the fault segments in the Oquirrh Mountain fault system are not fully linked together.

CONCLUSIONS

The South Oquirrh Mountain normal fault zone consists of four fault strands. Geometrically, these faults are arranged in a right-stepping pattern in the north and a left-stepping pattern in the south, with the West Mercur fault forming the central part. Thus, the fault zone is convex-shaped in map view for a distance of 25 km. Late Quaternary fault activity is characterized by 2.0–4.5 m high discontinuous fault scarps developed in both late Quaternary alluvium and bedrock. The fault scarps in bedrock contain evidence of two rupture events. The maximum surface offset measured across the scarps occurs close to the apex of the convex-shaped fault zone, where the West Mercur fault is located. The last surface rupturing occurred prior to the highstand of Lake Bonneville (15 ka). Characteristics of cumulative displacement inferred from range crest elevations, Bouguer gravity data in the adjacent basin, and rotation of the secondary faults adjacent to the West Mercur fault are consistent with those of displacements measured across late Quaternary fault scarps. The maximum displacement is near the apex of the convex-shaped fault zone and then tapers off towards both ends of the fault zone.

Surface fault traces that range from a few meters to tens of kilometers long are characterized by two dominant orientations (strikes N11°W and N43°W), separated by an angle of 33° ± 5°. Slip directions concentrate on a trend of S70°W, perpendicular to the average strike of the fault zone. Thus, it appears that the geometry of the fault surfaces is composed of self-similar structural ridges and furrows of variable wavelength and amplitude that are elongated parallel to the slip direction.

The relationships between fault geometry, displacement and geomorphology in the South Oquirrh Mountains fault zone suggest a growth model of normal faults in which the apex of the convex-shaped fault sections mark the nucleation points of fault zones. Newly-formed secondary faults developed at both ends of the primary fault step into the footwall as the fault zone grows laterally. Large concave or 'cuspate' fault sections mark sites where the independently nucleated faults join together.

Acknowledgements—Support for this research was provided by NSF grants EAR-8721100, EAR-9104677 and Sigma Xi. Daning Wu was partly supported at the University of Utah by grant EAR-872110, which is part of a co-operative National Science Foundation exchange program with the State Seismological Bureau of the People's Republic of China. We thank Jennifer Helm for her care and patience in editing earlier versions of the manuscript. Discussion with John Bartley on technical issues concerning normal faulting were particularly helpful. We also thank Susan Olig for reviewing the manuscript prior to submittal. W. L. Power and S. F. Personius provided excellent critical reviews of the original manuscript.

REFERENCES

Bankey, V., Webring, M., Mabey, D. R., Kleinkopf, M. D. & Bennett, E. H. 1985. Complete Bouguer gravity anomaly map of Idaho. *U.S. geol. Surv. Misc. Field Studies Map* **MF-1773**, scale 1:500,000.

Bakun, W. H., Stewart, R. M., Bufe, C. G. & Marks, S. M. 1980. Implication of seismicity for failure of a section of the San Andreas fault. *Bull. seism. soc. Am.* **70**, 185–201.

Barnhard, T. P. 1988. Fault-scarp studies of the Oquirrh Mountains, Utah. In: *In the Footsteps of G. K. Gilbert—Lake Bonneville and Neotectonics of the Eastern Basin and Range Province* (edited by Machette, M. N.) *Utah Geol. Min. Surv. Misc. Publ.* **88-1**, 52–54.

Barnhard, T. P. & Dodge, R. L. 1988. Map of fault scarps formed on unconsolidated sediments, Tooele 1° × 2° quadrangle, northwestern Utah. *U.S. geol. Surv. Misc. Field Studies Map* **MF-1990**, scale 1:250,000.

Barnsley, M. F., R. L. Devaney, B. B. Mandelbrot, H.-O. Peitgen, D. Saupe & R. F. Voss. 1988. *The Science of Fractal Images*. Springer, New York.

Bonilla, M. G., Mark, R. K. & Leinkaemper, J. J. 1984. Statistical relations between earthquake magnitude, surface rupture length, and surface fault displacement. *Bull. seism. soc. Am.* **74**, 2379–2411.

Bruhn, R. L., Gibler, P. R. & Parry, W. T. 1987. Rupture characteristics of normal faults: an example from the Wasatch fault zone, Utah. In: *Continental Extensional Tectonics* (edited by Coward, M. P., Dewey, J. F. & Hancock, P. L.). *Spec. Publs geol. Soc. Lond.* **28**, 337–353.

Bruhn, R. L. 1992. Structure of normal fault zones in the western U.S. *Geol. Soc. Am. Prog. w. Abs.* **23**, 68.

Bucknan, R. C. & Anderson, R. E. 1979. Estimation of fault-scarp ages from a scarp-height-slope-angle relationship. *Geology* **7**, 11–14.

Cook, K. L., Bankey, V., Mabey, D. R. & DePangher, M. 1989. Complete Bouguer Gravity Anomaly Map of Utah. *Utah Geol. Min. Surv. Misc. Publ.* **122**.

Cowie, P. A. & Scholz, C. H. 1991. Physical explanation for displacement–length relationship for faults using a post-yield fracture mechanics model. *J. Struct. Geol.* **14**, 1133–1148.

Crone, A. J., Machette, M. N., Bonilla, M. G., Lienkaemper, J. L., Pierce, K. L., Scott, W. E. & Bucknam, R. C. 1987. Surface faulting accompanying the Borah Peak earthquake and segmentation of the Lost River fault, central Idaho. *Bull. seism. soc. Am.* **77**, 739–770.

Crone, A. J. & Haller K. M. 1991. Segmentation and the coseismic behavior of Basin and Range normal faults: examples from east-central Idaho and southwestern Montana, U.S.A. *J. Struct. Geol.* **13**, 151–164.

Currey, D. R. & Oviatt, C. G. 1985. Duration, average rates, and probable causes of Lake Bonneville expansions, stillstands, and contractions during the last deep-lake cycle, 32,000 to 10,000 years ago. In: *Problems of and Prospects for Predicting Great Salt Lake Levels: Center for Public Affairs and Administration* (edited by Kay, P. A. & Diaz, H. F.). University of Utah, Salt Lake City, 9–24.

Currey, D. R. 1990. Quaternary paleolakes in the evolution of semidesert basins with special emphasis on Lake Bonnevile and the Great Basin, U.S.A. *Palaeogeogr., Paleoclim., Palaeoec.* **76**, 189–214.

Eaton, J. P., O'Neill, M. E. & Murdock, J. N. 1970. Aftershocks of 1966 Parkfield-Cholame earthquake: A detailed study. *Bull. seism. soc. Am.* **60**, 1151–1197.

Everitt, B. L. & Kaliser, B. N. 1980. Geology for assessment of seismic risk in the Tooele and Rush Valleys, Tooele County, Utah. *Utah Geol. Min. Surv. Spec. Stud.* **51**.

Gibson, J. R., Walsh, J. J. & Watterson, J. 1989. Modelling of bed contours and cross-sections adjacent to planar normal faults. *J. Struct. Geol.* **11**, 317–328.

Gilbert, G. K. 1890. Lake Bonneville. *U.S. geol. Surv. Monogr.* **1**.

Gilluly, J. 1928. Basin Range faulting along the Oquirrh Range, Utah. *Bull. geol. Soc. Am.* **39**, 1103–1130.

Gilluly, J. 1929. Possible desert-basin integration in Utah. *J. Geol.* **37**, 672–682.

Gilluly, J. 1932. Geology and ore deposits of the Stockton and Fairfield Quadrangles, Utah. *Prof. Pap. U.S. geol. Surv.* **173**.

Gilluly, J. 1967. Chronology of tectonic movements in the western United States. *J. Am. Sci.* **265**, 306–331.

Guilbert, J. M. & Park C. F. 1986. *The Geology of Ore Deposits*. W. H. Freeman, New York.

Hintze, L. F. 1982. Geologic history of Utah. *Brigham Young University Geol. Stud.* **20**.

Hunt, C. B. 1982. Pleistocene Lake Bonneville, ancestral Great Salt Lake, as described in the notebooks of G. K. Gilbert, 1875–1880. *Brigham Young University Geol. Stud.* **29**.

King, G. C. P. 1986. Speculations on the geometry of the initiation and termination process of earthquake rupture and its relation to morphology and geological structure. *Pure & Appl. Geophys.* **124**, 567–585.

Machette, M. N. 1984. Preliminary investigations of late Quaternary slip rates along the southern part of the Wasatch fault zone, central Utah. In Hays, W. W. and Gori, P. L., eds, *Proceedings of Workshop on Evolution of Regional and Urban Earthquake Hazards and Risk in Utah, Salt Lake City, Utah*, 14–16 August 1984 (edited by Hays, W. W. & Gori, P.). *U.S. geol. Surv. Open-file Rep.* **84-763**, 391–406.

Machette, M. N. 1989. Slope-morphometric dating. In: *Dating Methods Applicable to Quaternary Geologic Studies in the Western United States* (edited by Forman, S. L.). *Utah Geol. Min. Surv. Misc. Publ.* **89-7**, 30–42.

Machette, M. N., Personius, S. F. & Nelson, A. R. 1991. The Wasatch fault zone, Utah—segmentation and history of Holocene earthquakes. *J. Struct. Geol.* **13**, 137–150.

Mandelbrot, B. B. 1983. *The Fractal Geometry of Nature*. W. H. Freeman, New York.

Masiha, L. & Smylie, D. E. 1971. The displacement fields of inclined faults. *Bull. seism. soc. Am.* **61**, 1433–1440.

Mason, D. B. 1992. Earthquake magnitude potential of active faults in the intermountain seismic belt from surface parameter scaling. Unpublished Master thesis, University of Utah.

Nelson, A. R. & Personius, S. F. 1990. Surficial geologic map of the Weber segment, Wasatch fault zone, Weber and Davis Counties, Utah. *U.S. geol. Surv. Misc. Invest. Map* **I-2099**, scale 1:50,000.

Olig, S. S., Lund, W. R. & Black, B. D. 1993. Evidence for mid-Holocene surface rupture on the Oquirrh fault zone. *GSA Cordilleran–Rocky Mountain Sec. Meeting Prog. w. Abs.* **129**.

Okubo, P. G. & Aki, K. 1987. Fractal geometry in the San Andreas fault system. *J. geophys. Res.* **92**, 345–355.

Pierce, K. L. & Coleman, S. M. 1986. Effect of height and orientation (microclimate) on geomorphic degration rates and processes, late-glacial terrace scarps in central Idaho. *Bull. geol. Soc. Am.* **97**, 860–885.

Power, W. L. & Tullis, T. E. 1991. Euclidean and fractal models for the description of rock surface roughness. *J. geophys. Res.* **96**, 415–423.

Reasenberg, P. & Ellsworth, W. L. 1982. Aftershocks of the Coyote Lake, California, earthquake of August 6, 1979: A detailed study. *J. geophys. Res.* **87**, 10,637–10,655.

Reches, Z. 1983. Faulting of rocks in three-dimensional strain fields. II. theoretical analysis. *Tectonophysics* **95**, 133–156.

Reches, Z. & Dieterich, J. H. 1983. Faulting of rocks in three-dimensional strain fields. I. Failure of rocks in polyaxial, servo-control experiments. *Tectonophysics* **95**, 111–132.

Rigby, J. K. 1958. Geology of the Stansbury Mountains, in Geology of the Stansbury Mountains. *Utah Geol. Soc. Guidebook* **13**, 1–134.

Savage, J. C. & Hastie, L. M. 1966. Surface deformation associated with dip-slip faulting. *J. geophys. Res.* **71**, 4897–4904.

Sibson, R. H. 1985. Stopping of earthquake rupture as dilational fault jogs. *Nature* **316**, 248–251.

Sibson, R. H. 1987. Effects of fault heterogeneity on rupture propagation. *U.S. geol. Surv. Open-file Rep.* **87-673**, 362–373.

Slemmons, D. B. 1957. Geological effects of the Dixie Valley–Fairview Peak, Nevada, earthquake of December 16, 1954. *Bull. seism. soc. Am.* **47**, 353–375.

Slemmons, D. B. 1977. Faults and earthquake magnitude. Vicksburg, Mississippi. *U.S. Army Corp of Engrs, Water. Exp. Sta. Misc. Pap.* **S-73-2**.

Scott, W. E., McCoy, W. D., Shrod, R. R. & Rubin, M. 1983. Reinterpretation of the exposed record of the last two cycles of Lake Bonneville, western United States. *Quat. Res.* **20**, 261–285.

Susong, D. D., Janecke, S. U. & Bruhn, R. L. 1990. Structure of a fault segment boundary in the Lost River fault zone, Idaho, and possible effect on the 1983 Borah Peak earthquake rupture. *Bull. seism. soc. Am.* **80**, 57–68.

Wallace, R. E. 1984. Faulting related to the 1915 earthquakes in Pleasant Valley, Nevada. *Prof. Pap. U.S. geol. Surv.* **1274**.

Walsh, J. J. & Watterson, J. 1988. Analysis of the relationship between displacements and dimensions of faults. *J. Struct. Geol.* **10**, 239–247.

Walsh, J. J. & Watterson, J. 1989. Displacement gradients on fault surfaces. *J. Struct. Geol.* **11**, 307–316.

Watterson, J. 1986. Fault dimensions, displacement and growth. *Pure & Appl. Geophys.* **124**, 365–373.

Wright, L. 1977. Late Cenozoic fault patterns and stress fields in the Great Basin and westward displacement of the Sierra Nevada block. *Geology* **4**, 489–494.

Wu, D. 1993. Geometry of active normal faults: implications for fault growth, earthquake rupturing, and landforms. Unpublished Ph.D. dissertation, University of Utah.

Zoback, M. L. 1983. Structure and Cenozoic tectonism along the Wasatch fault zone, Utah. In: *Tectonic and Stratigraphic Studies in the Eastern Great Basin* (edited by Miller, D. M., Todd, V. R. & Howard, K. A.). *Mem. geol. soc. Am.* **157**, 3–28.